Proceedings of the Combustion Institute 41 (2025) 105828

Contents lists available at ScienceDirect

Proceedings of the Combustion Institute

journal homepage: www.elsevier.com/locate/proci

Acetaldehyde reactivity at engine-relevant conditions: An experimental and kinetic modeling study

Jesus Caravaca-Vilchez *, Malte Döntgen, Karl Alexander Heufer

Chair of High Pressure Gas Dynamics, Shock Wave Laboratory, RWTH Aachen University, Aachen, 52056, Germany

ARTICLE INFO

Keywords:
Acetaldehyde
Rapid compression machine
Shock tube
Negative temperature coefficient
Kinetic modeling

ABSTRACT

Understanding the combustion chemistry of acetaldehyde, a carcinogenic by-product formed during the low-temperature oxidation of various hydrocarbons, is essential for reducing harmful emissions in engines. Previous acetaldehyde experimental works have largely focused on low-pressure conditions, with a few exceptions. Some studies report a clear negative temperature coefficient (NTC) behavior for acetaldehyde and highlight the need for further low-temperature, high-pressure experiments to fully characterize it. In this context, acetaldehyde ignition delay times were measured using a rapid compression machine and a shock tube over a wide range of conditions (580–1410 K, 10–40 bar, and equivalence ratios of 0.5–1.5), significantly extending the very limited IDT data available in the literature at 10 bar. At low temperatures, the most comprehensive kinetic models of acetaldehyde greatly underestimate its reactivity, even those that show reasonable performance for flow reactor species measurements from the literature in the same temperature regime. At high temperatures, model predictions were generally in better agreement with the measured data. To improve prediction accuracy, refinements were made within GalwayMech1.0 model, incorporating recently calculated thermochemistry from the literature and modified reaction rate parameters based on direct analogies and literature information. The resulting chemistry revealed that the acetyl peroxy radical is the primary driver of low-temperature reactivity at high pressures through a closed-loop fuel consumption pathway. Further adjustments in the peroxyl radicals chemistry, which is less relevant under low-pressure conditions, successfully separate first-stage and main ignition in the NTC region. At high temperatures, revised H-atom abstraction by $\dot{H}$ and O_2 rates improved high-temperature predictions. Overall, the proposed model outperforms existing mechanisms over a wide range of conditions, but retains uncertainties in the formation of a few minor intermediates. This work highlights the importance of using high-pressure validation targets for comprehensive kinetic modeling and provides a solid foundation for future studies on acetaldehyde oxidation.

1. Introduction

Acetaldehyde is a carcinogenic compound with significant health risks. It is formed during the low-temperature oxidation of various hydrocarbons [1–5]. A comprehensive understanding of acetaldehyde oxidation and pyrolysis is critical to the development of effective emission control strategies for internal combustion engines. Over the years, acetaldehyde combustion has been examined using various experimental techniques, including ignition delay time (IDT) measurements in rapid compression machines (RCM) [6,7] and shock tubes (ST) [8–13], species concentration analysis in static [14], jet-stirred (JS) [9,15,16] and plug flow reactors (PFR) [17,18], pyrolysis investigations [19,20], molecular beam mass spectrometry in low-pressure laminar premixed flames [21,22], and laminar flame speed measurements [23]. Some of these works [7,13,16,18] also developed comprehensive kinetic models for acetaldehyde oxidation at a wide range of conditions. The findings of most of these studies are explicitly summarized in the recent study from Ren et al. [24]. They refined a detailed kinetic model from the literature [7] using least squares methods on key kinetic parameters in acetaldehyde combustion and highlighted the need for further optimization using experimental data.

Most of the experimental data available in the literature pertain to low-pressure conditions, with the exception of the studies by Hashemi et al. [18], Tao et al. [7], Griffiths et al. [6] and Dagaut et al. [9]. Hashemi et al. [18] explored the oxidation of acetaldehyde at high pressures ranging from 25 to 100 bar at 600–900 K, using a PFR at lean, highly diluted conditions. Their results showed a negative temperature coefficient (NTC) behavior in the investigated regime. This behavior was previously observed in low-pressure JSR studies [15,16], where it

* Corresponding author.
E-mail address: caravaca_vilchez@hgd.rwth-aachen.de (J. Caravaca-Vilchez).

https://doi.org/10.1016/j.proci.2025.105828
Received 28 April 2025; Accepted 30 August 2025
Available online 20 September 2025

was attributed to the competition between acetyl radical decomposition and its addition to O_2. Hashemi et al. [18] further supported this interpretation by proposing that the NTC behavior at high pressures is strongly affected by the chemistry of peroxyl species.

The early work of Griffiths et al. [6] first conducted IDT experiments at pressures up to 10 bar for acetaldehyde/air mixtures ($0.2 \leq \phi \leq 1$) in an RCM. They observed a clear two-stage ignition at 610–775 K. More recently, Tao et al. [7] measured IDTs in an RCM under stoichiometric conditions at similar pressures but higher temperatures (730–1100 K) and a greater dilution. Unlike Griffiths et al. [6], they observed first-stage (FS) heat release before the end of compression below 800 K, leading the authors to exclude this data from their kinetic analysis. Tao et al. [7] attributed the NTC behavior in the RCM regime to the fate of ethane formed by methyl radical recombination. They also emphasized the need for further experimental studies in the low-temperature, high-pressure regime to fully understand the NTC behavior of acetaldehyde.

In the early 1990s, Dagaut et al. [9] investigated the high-temperature oxidation of acetaldehyde in a JSR at 900–1300 K and pressures up to 10 atm. They also measured IDTs in a ST across a wide range of fuel/O_2 ratios ($0.5 \leq \varphi \leq 2$) and temperatures (1230–2530 K), at pressures from 2 to 5 bar. To the authors' knowledge, no other IDT measurements in STs have been reported at higher pressures to date. Given the incomplete understanding of NTC behavior and the scarcity of high-pressure experimental data across the full temperature range, this study extends IDT measurements using a ST and an RCM at 10, 20, and 40 bar (with 40 bar data exclusive to the RCM) over temperatures from 580 to 1413 K for lean, stoichiometric, and rich mixtures (φ = 0.5, 1.0 and 1.5). The performance of the most comprehensive acetaldehyde kinetic models from the literature was evaluated using the new experimental data. A kinetic model incorporating a well-validated base chemistry, GalwayMech1.0, was updated based on a wide set of validation targets using reaction rate analogies and literature information. Key reaction pathways were analyzed to gain a deeper insight into the combustion behavior of acetaldehyde at high pressures. The proposed model was comprehensively validated against the present measurements and literature data.

2. Facilities description

For the investigation of IDTs, two facilities at RWTH Aachen University were utilized: a diaphragmless ST and a single-piston RCM. Detailed descriptions of both facilities are available in [25,26] and only a brief overview is provided here.

2.1. Shock tube

The ST consists of a 4.5 L barrel-shaped driver section and a 6.0 m driven section with an inner diameter of 45 mm. The diaphragmless operation is facilitated by a two-piston valve, based on the design by Oguchi et al. [27]. A helium/air mixture was used as the driver gas, with the ratio of gases optimized to achieve the desired shock velocities while minimizing shock contact surface interaction effects. Incident shock velocities were measured over the last 3.6 m of the driven section using five silicon-coated KISTLER pressure transducers (603B, 6005) and a PCB 113B22 sensor. IDTs were defined as the time between the arrival of the reflected shock at the closest sidewall pressure sensor (PCB), located 12 mm from the end wall, and the steepest pressure rise induced by autoignition. Gas conditions behind the reflected shock were determined using an in-house code based on the "Shock and Detonation Toolbox" [28] for Cantera [29]. All experiments were conducted without external heating. However, four type-T thermocouples were used to verify the uniformity of the initial temperature distribution across the ST. Experimental uncertainties were determined using the procedure described in [30], yielding ±0.7% for temperature and ±1.5% for pressure.

Table 1
Overview of the investigated conditions.

φ [−]	Dilution [dil./O2]	p [bar]	T [K]
0.5	8.875	10, 20, 40	580–1390
1.0	13	10, 20	580–1415
1.5	13	20	575–1380

2.2. Rapid compression machine

The RCM operates as a single-piston system with a creviced design to suppress roll-up vortex formation. It features a reactor chamber with an adjustable end wall, allowing modulation of the compression ratio and precise control of the compression temperature at constant initial temperature (30 °C). Different bath gas compositions are used to extend the accessible test temperature range. A Kistler 6125C11U20 pressure sensor was used to monitor pressure variations within the reactor. In the RCM, IDTs are determined as the interval between the end of compression (EOC) and the maximum pressure rise rate associated with the main autoignition event and, if present, the FS ignition. The EOC temperature is derived from isentropic compression relations using the measured pressure under the adiabatic core assumption. The uncertainties in the EOC pressure and temperature are estimated to be ±0.5% and ±1% respectively, corresponding to an uncertainty of about 25% in IDTs, as reported by Büttgen et al. [31].

2.3. Simulation methods

IDT simulations were performed with custom scripts using Cantera [29]. For IDT experiments not exceeding 2 ms, simulations were performed under a constant-volume assumption. For longer IDTs, non-reactive experiments were conducted to account for facility effects. These include small pressure perturbations due to shock contact surface interaction in the ST, and compression and heat loss phases in the RCM. In these experiments, oxygen (O_2) was replaced by nitrogen (N_2) and the resulting pressure trace was used to derive an effective volume profile which was then prescribed in the quasi-0D simulation [32]. The non-reactive volume profiles are provided in the Supplementary Material (SM).

2.4. Mixture preparation

For both facilities, acetaldehyde (99.5%) and high purity grade gases (99.999%) of O_2, N_2, argon (Ar) and carbon dioxide (CO_2) were used for mixture preparation in separate stainless-steel vessels, with composition control achieved by monitoring the partial pressures of all components. Given acetaldehyde's propensity to polymerize [6], higher dilution levels were required in the studied mixtures to ensure their stability during the experiments. The mixtures were periodically analyzed in a gas chromatography/mass spectrometry system [5], confirming negligible acetaldehyde loss and no formation of other species after 3 h for partial pressures below 130 mbar. Despite the need for dilution, the initial fuel concentrations in the investigated mixtures remained higher (up to 4.1%) than those used in recent high-pressure acetaldehyde oxidation studies (up to 2.7%) [7,18]. A summary of the investigated conditions is presented in Table 1. These conditions were adjusted to match the experimental limits of the facilities. For example, in the 20 bar, φ = 1.5 dataset, no measurements are provided between 670 and 770 K. In the ST, shock contact wave interactions effects compromised data quality below 770 K, while in the RCM, the high reactivity above 670 K led to ignition delays shorter than 3 ms, preventing a clear definition of the end of compression. Despite these limitations, the combined RCM and ST datasets form a reliable foundation for investigating the NTC behavior of acetaldehyde. The measured data is provided in the SM.

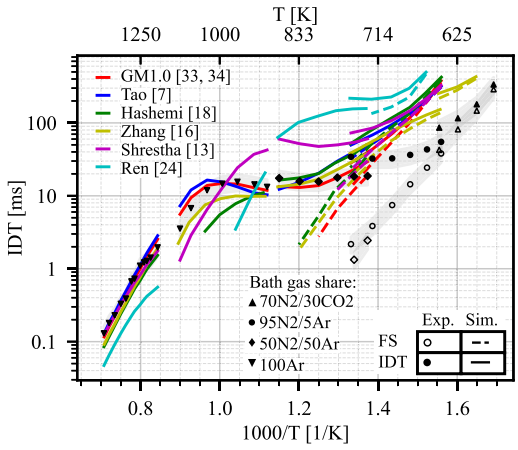

Fig. 1. Comparison of different literature models against measured IDTs at 10 bar and $\varphi = 1$. Shadow areas indicate the uncertainty in the measurements.

3. Model comparison

The five most comprehensive kinetic models from the literature for acetaldehyde combustion—developed by Zhang et al. [16], Tao et al. [7], Hashemi et al. [18], Shrestha et al. [13] and Ren et al. [24]—were evaluated against the present data. An additional model, GalwayMech1.0 (GM1.0) [33,34], was added as benchmark due to its extensive validation for smaller species relevant in the oxidation of acetaldehyde (like methanol, methane or hydrogen). Fig. 1 compares model predictions with measured data at 10 bar and $\varphi = 1$. Variations in bath gas composition induce a discontinuous change in the compression ratio, leading to the observed jump in measured IDTs in the RCM. Additional comparisons for the conditions listed in Table 1 are provided in the SM.

In the high-temperature range (1100–1400 K), the experimental data show an Arrhenius trend. With the exception of Ren's model, which significantly overpredicts reactivity, all models show reasonable agreement in this regime where literature data already exist at low pressures. Below 1100 K, the temperature-IDT curve exhibits a wide S-shaped plateau, characteristic of NTC behavior. Below 870 K, a two-stage ignition is observed. Between 740 K and 870 K, FS heat release occurs before EOC, in agreement with observations by Tao et al. at comparable conditions [7]. To improve the readability of the IDT plots, the effect of this early heat release on the test temperature is ruled out by plotting both measured and simulated data against the temperature determined from the non-reactive pressure trace obtained for each condition. In the temperature range of 740–1100 K, GM1.0 is the only model that reasonably captures reactivity, whereas most models predict shorter IDTs at high temperatures and longer ones in the NTC region compared to experimental observations. Tao's model accurately predicts IDTs only within its original validation range (800–1100 K), but deviates elsewhere.

As temperature decreases below the NTC minimum (< 740 K), the FS shifts towards the main ignition, which is consistent with previous RCM experiments [6]. In this temperature regime, where the Zhang and Hashemi models showed reasonable performance against flow reactor low-pressure or low-reactant-concentration species measurements [16,18], all models significantly underpredict reactivity at the investigated conditions. Notably, no ignition was observed in the simulated pressure traces by most models for $T < 660$ K, except for Zhang's. Besides, all models predict FS ignition much closer to the main ignition than observed experimentally. These findings suggest a fundamental gap in the understanding of acetaldehyde NTC behavior at high pressures, highlighting the need for improved kinetic modeling.

4. Kinetic modeling

4.1. Model description

In this study, updates to the combustion chemistry of acetaldehyde were implemented into GalwayMech1.0 (GM1.0) [33,34]. The development of this model follows a hierarchical structure from hydrogen/O_2 to n-heptane chemistry. A reduced version of GM1.0, limited to C_3 species, serves as the base mechanism in this work.

The acetaldehyde combustion chemistry in this model, originally developed by Pelucchi et al. [35], has been refined by Curran's group over the years, incorporating recently calculated kinetic parameters. However, previous studies have shown that such parameters often need to be optimized by experimental validation, as highlighted in Section 3. In this context, the rate constants of 21 reactions within the acetaldehyde submechanism were updated using literature values and analogies with similar molecules. In addition, the alkane-like low-temperature chemistry pathway proposed by Zhang et al. [16] was incorporated into the model. It involves five-membered ring isomerization of the acetyl peroxy radical, followed by a second addition to O_2, ketohydroperoxide formation, and subsequent decomposition ($CH_3C\dot{O}_3 \Leftrightarrow \dot{C}H_2CO_3H \Leftrightarrow \dot{O}_2CH_2CO_3H \Leftrightarrow KHO_2COCHO + \dot{O}H \Leftrightarrow CO_2 + H\dot{C}O + \dot{O}H$). Besides, the thermochemistry of key species within the acetaldehyde submechanism relevant to its NTC region has been updated using the recent ab initio calculations from Shrestha et al. [13]. This includes formyl methyl radical ($\dot{C}H_2CHO$), its peroxy radical ($\dot{O}_2CH_2CHO$) and the corresponding isomerization product ($HO_2CH_2\dot{C}O$). The species dictionary and the proposed kinetic model are available in the SM.

Table 2 provides a comprehensive list of the modified reactions and their corresponding rate sources. The reasoning behind every change will be detailed in the following sections. All proposed modifications remain within the expected uncertainty ranges of the previously assigned parameters and are smaller than the standard uncertainties associated with ab initio methods. A comparison of the modified kinetic parameters with literature values is available in the SM.

4.2. Kinetic analysis

In this section, the main reaction pathways involved in the oxidation of acetaldehyde are discussed. Pathway analyses were performed at $\varphi = 1$ and 10 bar across the full temperature range studied. Four representative temperatures were chosen: 600 and 800 K (Fig. 2), and 1200 and 1400 K (Fig. 4). For a deeper understanding of reaction rate influences, detailed sensitivity analyses are provided in the SM.

4.2.1. Low-temperature regime

At temperatures below the NTC minimum, acetaldehyde primarily undergoes H-atom abstraction (HAA) at the carbonyl site (α-position) forming acetyl radicals ($CH_3\dot{C}O$), mainly by acetyl peroxy radicals ($CH_3C\dot{O}_3$) and, to a lower extent, by methoxy ($CH_3\dot{O}$) and hydroxyl ($\dot{O}H$) radicals. Note that HAA at the methyl site (β-position) is less favored in this temperature range due to the higher C-H bond dissociation energy (BDE ≈ 100 kcal/mol) compared to the α-position (BDE ≈ 89 kcal/mol). $CH_3\dot{C}O$ then adds to O_2, forming $CH_3C\dot{O}_3$, while its decomposition to methyl radical ($\dot{C}H_3$) and carbon monoxide (CO) plays only a minor role at the low-temperature, high-O_2-concentration conditions investigated in this work. The major consumption pathways of $CH_3C\dot{O}_3$ at 600 K (see Fig. 2) are: (1) HAA at the α-position of the fuel, forming peracetic acid (CH_3CO_3H), which decomposes rapidly to $\dot{O}H$ and an alkoxy radical ($CH_3C\dot{O}_2$) and (2) $R\dot{O}_2 + R\dot{O}_2$ type reactions [43], direcly forming $CH_3C\dot{O}_2$, $CH_3\dot{O}$ and O_2. $CH_3C\dot{O}_2$ further decomposes into CO_2 and $\dot{C}H_3$. Overall, $CH_3\dot{C}O$ decomposition and pathways (1) and (2) ultimately lead to $\dot{C}H_3$ formation. The key difference among these pathways is that (1) involves fuel consumption and $\dot{O}H$ production, whereas (2) and $CH_3\dot{C}O$ decomposition do not generate additional reactive radicals. Therefore, (1) is the most

Table 2
Modified reactions in this work.

N°	Reaction	Source
1	CH3CHO + O2 ⇔ CH3CO + HO2	[36]
2	CH3CHO + OH ⇔ CH3CO + H2O	[37]/2
3	CH3CHO + OH ⇔ CH2CHO + H2O	[38]
4	CH3CHO + HO2 ⇔ CH3CO + H2O2	[39]/1.5
5	CH3CHO + CH3O2 ⇔ CH3CO + CH3O2H	[16] × 2.5
6	CH3CHO + CH3CO3 ⇔ CH3CO + CH3CO3H	[16] × 2.5
7	CH3CHO + CH3O ⇔ CH3CO + CH3OH	[16]/2
8	CH3CO + O2 ⇔ CH2CO + HO2	[40]
9	CH3CO + O2 ⇔ CH3CO3	a
10	CH3CO ⇔ CH3 + CO	[41] × 1.3
11	CH3CO3 + HO2 ⇒ CH3CO2 + OH + O2	[42]
12	CH3CO3 + HO2 ⇔ CH3CO3H + O2	[42]
13	CH3CO3 + CH3O2 ⇒ CH3CO2 + CH3O + O2	b
14	CH3CO3 + CH3O2 ⇒ CH3COOH + CH2O + O2	[43]
15	CH3CO3 + CH4 ⇔ CH3CO3H + CH3	[13]
16	CH3CO3 + CH3CO3 ⇒ 2 CH3CO2 + O2	b
17	CH3CO3H ⇔ CH3CO2 + OH	[36]
18	CH3CHO + H ⇔ CH3CO + H2	c
19	CH3CHO ⇔ CH3 + HCO	[12]
20	CH2CHO ⇔ CH3 + CO	[41]
21	CH2CHO + HO2 ⇒ HCO + CH2O + OH	[13] tablenotes

a: Pressure dependence [44], high-pressure limit [24].
b: Alkanes analogy. c: Refitted rate.

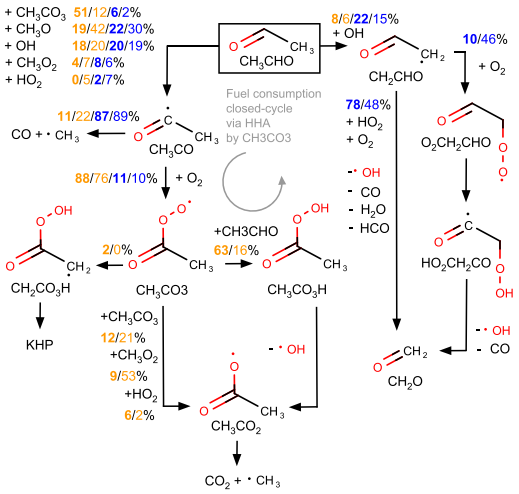

Fig. 2. Reaction pathway analysis when 10% of the fuel is consumed using proposed (bold) and original (normal) models at 10 bar, $\varphi = 1$, 600 K (orange) and 800 K (blue). Names below the structures follow the mechanism naming scheme.

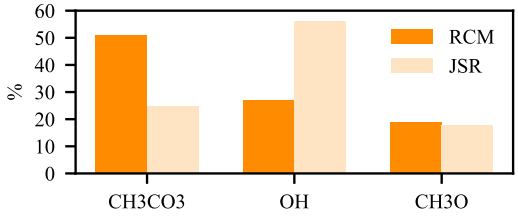

Fig. 3. Percentage contributions of the most relevant HAA reactions to acetaldehyde consumption at 600 K and $\varphi = 1$, for RCM (10 bar, 2.8% CH_3CHO) and JSR (1 bar, 2% CH_3CHO [16]) conditions, using the present model.

reactivity-enhancing pathway, whereas (2) and especially $CH_3\dot{C}O$ decomposition are the most important reactivity-inhibiting pathways at low temperatures (see Fig. S6 from SM). In contrast, the conventional low-temperature chain branching pathway adopted from Zhang [16] (KHP) shows smaller impact on reactivity due to the low flux into this channel at the investigated conditions.

The low-temperature oxidation chemistry of acetaldehyde differs substantially from that of alkanes. In propane, HAA by $\dot{O}H$, rather than by its corresponding $R\dot{O}_2$ species, is the dominant consumption pathway at comparable conditions [45]. While $R\dot{O}_2$ species formation is significant in both cases, C–H bond strengths differ substantially between the two molecules. Propane shows relatively strong C-H bonds (BDE ≈ 97–100 kcal/mol), making HAA less favorable and facilitating alternative $R\dot{O}_2$ species consumption routes, such as internal H-atom isomerization followed by chain-branching reactions and concerted eliminations [45]. In contrast, acetaldehyde exhibits a notably weaker C–H bond at the α-position (BDE ≈ 89 kcal/mol), thereby favoring HAA as the primary $R\dot{O}_2$ consumption pathway. Overall, the high production of $CH_3C\dot{O}_3$ at these conditions, combined with the weak C–H bond dissociation energy at the carbonyl site, result in HAA by $CH_3C\dot{O}_3$ being the most significant pathway for fuel consumption, despite the HAA by $\dot{O}H$ rate constant being four orders of magnitude higher (see Fig. S8 in the SM). However, as pressure and/or initial fuel molar fraction decrease, the resulting lower O_2 concentration limits $CH_3C\dot{O}_3$ formation via $CH_3\dot{C}O$ addition to O_2, favoring $CH_3\dot{C}O$ decomposition instead. Therefore, acetaldehyde consumption at JSR conditions is rather dominated by HAA by $\dot{O}H$, as illustrated in Fig. 3.

Given the tendency of GM1.0 to underpredict reactivity at low temperatures, pathway (1) was enhanced (see Fig. 2) by increasing HAA by $CH_3C\dot{O}_3$ and CH_3CO_3H decomposition, and decreasing $R\dot{O}_2$ + $R\dot{O}_2$ reaction rates, the latter by about an order of magnitude. The original $R\dot{O}_2$ + $R\dot{O}_2$ rates were extrapolated from atmospheric measurements, whereas in this work a direct analogy to the methyl peroxy radical self-reaction ($CH_3\dot{O}_2$ + $CH_3\dot{O}_2$) rate proposed in [46] was adopted. This rate was calculated between 600 and 719 K—closer to the temperature range investigated in the present study—and has been consistently adopted in the original mechanism for analogous C_2 and C_3 reactions [47]. These modifications significantly decreased the IDTs at low temperatures, but also undesirably increased fuel consumption and the formation of key intermediates such as H_2O and CO_2 at low-pressure JSR conditions. To mitigate this, HAA by $\dot{O}H$ and $CH_3\dot{O}$ at the α-position was reduced, as they have minimal impact on reactivity at high pressures. In addition, $CH_3\dot{C}O$ consumption pathways were adjusted by slighly increasing the decomposition reaction rate and updating the pressure dependence of addition to O_2 to reduce its effect at low pressures.

4.2.2. NTC regime

With increasing temperature, HAA at the β-position forming $\dot{C}H_2CHO$ becomes relevant due to its higher C-H bond strength, while the contribution of HAA by $CH_3C\dot{O}_3$ diminishes as $CH_3C\dot{O}$ preferentially undergoes decomposition, leading to $\dot{C}H_3$ and CO, rather than addition to O_2 (see Fig. 2, 800 K). Meanwhile, the formation of smaller peroxyl radicals is promoted via: (1) The increased build-up of $\dot{C}H_3$, which facilitates $CH_3\dot{O}_2$ formation via addition to O_2. (2) The higher production of $\dot{C}H_2CHO$, which further produces formaldehyde (CH_2O). CH_2O chemistry is the primary source of hydroperoxyl radicals ($H\dot{O}_2$) at these temperatures via formyl radical ($H\dot{C}O$) reaction with O_2. The increased production of these peroxyl radicals (i.e. $CH_3\dot{O}_2$ and $H\dot{O}_2$) enhances reactivity by facilitating the formation of hydrogen peroxide and methyl hydroperoxide via fuel HAA reactions. These species further decompose into reactive radicals, i.e. $CH_3\dot{O}$ and $\dot{O}H$, at high temperatures. Notably, HAA by $CH_3\dot{O}_2$ and $H\dot{O}_2$ are the two most

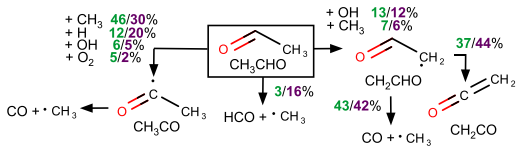

Fig. 4. Reaction pathway analysis when 10% of the fuel is consumed using the present model at 10 bar, φ = 1, 1200 K (green) and 1400 K (purple). Names below the structures follow the mechanism naming scheme.

reactivity-enhancing reactions at 800 K (see Fig. S7 in the SM). Overall, peroxyl radicals chemistry plays a key role in the NTC behavior at the studied conditions, whereas its influence is less pronounced under JSR conditions, where O_2 reactions are limited due to lower reactant concentrations.

In Section 3, it was noted that state-of-the-art kinetic models predict acetaldehyde FS ignitions much closer to main ignitions than observed experimentally. The low-temperature modifications introduced above affected both FS and main ignition similarly. However, they resulted in excessively short IDTs. During the transition from FS to total IDT, reactions involving $H\dot{O}_2$ become a major source of $\dot{O}H$. As a result, optimizing these reactions can have a significant effect on total IDTs, while minimally affecting FS ignitions. Therefore, the following changes in fuel-specific $H\dot{O}_2$ chemistry are proposed: (1) Increase of $CH_3C\dot{O}_3$ + $H\dot{O}_2$ reaction rates, and (2) decrease of fuel HAA by $H\dot{O}_2$ at the α-position and $\dot{C}H_2CHO$ + $H\dot{O}_2$ reaction rates. The updated thermochemistry of Shrestha et al. [13] also contributes to this effect by shifting the $\dot{C}H_2CHO \Rightarrow \dot{O}_2CH_2CHO \Rightarrow HO_2CH_2\dot{C}O$ pathway towards reactants, thereby limiting CH_2O formation and consequently $H\dot{O}_2$ production. Modification (1) mainly affects the NTC minimum, where $CH_3C\dot{O}_3$ is still formed, while (2) and the thermochemical updates influence the entire NTC region plateau, causing undesired reactivity inhibition at the NTC maximum. To counteract this, fuel HAA at the α-position by $CH_3\dot{O}_2$ forming CH_3O_2H was increased. This change had less effect on the NTC minimum, because at lower temperatures CH_3O_2H consumption shifts from unimolecular chain-branching decomposition to chain-propagating HAA by $CH_3\dot{O}$.

4.2.3. High-temperature regime

The high-temperature oxidation of acetaldehyde has already been extensively studied [12]. At temperatures above the NTC maximum, HAA by $\dot{C}H_3$ becomes a major consumption pathway, while the contribution of $CH_3\dot{O}$ decreases (see Fig. 4, 1200 K). This can be explained by the reduced propensity for low-temperature methane chemistry (R + O_2, $R\dot{O}_2$ + $R\dot{O}_2$) that results in reduced $CH_3\dot{O}$ formation, allowing more $\dot{C}H_3$ to participate in the fuel HAA. Besides, HAA by hydrogen radicals ($\dot{H}$) becomes significant at higher temperatures due to the increased relevance of the $\dot{C}H_2CHO$ β-scission, which produces ketene and $\dot{H}$. Under these conditions, the most inhibiting reaction is HAA by $\dot{H}$, as it sequesters these radicals from branching pathways (e.g., $\dot{H}$ + $O_2 \Leftrightarrow \dot{O}$ + $\dot{O}H$). In contrast, the most reactivity-enhancing reaction is HAA by O_2 leading to $H\dot{O}_2$, thereby promoting high-temperature chain branching. At even higher temperatures (see Fig. 4, 1400 K), unimolecular acetaldehyde decomposition to $\dot{C}H_3$ and $H\dot{C}O$ becomes a major consumption route, promoting reactivity through $H\dot{O}_2$ formation ($H\dot{C}O$ + $O_2 \Leftrightarrow$ CO + $H\dot{O}_2$).

The overly steep slope of the IDT-temperature curve predicted by GM1.0 was slightly corrected by: (1) Increasing the rate of HAA by $\dot{H}$ to inhibit reactivity at temperatures above 1250 K, (2) increasing HAA by O_2 to shorten IDTs at temperatures below 1250 K. Modification (1) is supported by the improved model performance against literature flame speed measurements [23] (see SM). Besides, the pressure dependence of both fuel and $\dot{C}H_2CHO$ decompositions was revised to improve the IDT prediction accuracy of the model at low pressures and high temperatures.

5. Model validation

The present model has been validated across a wide range of conditions, including species measurements in JSR, PFR and flat premixed flames, as well as IDTs and laminar flame velocities. This section evaluates its performance against representative IDTs measured in this study and species data from the literature. Additional validation is provided in the SM.

Fig. 5 shows IDT data over a wide range of pressures and φ, measured in the ST and in the RCM. At high temperatures, the proposed model predicts a slightly less steep IDT-temperature dependence and generally agrees better with the experimental data than the original model. At lower temperatures, present model predictions are within experimental uncertainties for most conditions, except for a slight overprediction of reactivity at the NTC minimum for φ = 0.5 and 10 bar (red) and a slight underprediction at low temperatures for φ = 1.5 and 20 bar (green). The original model is excluded from this comparison due to its poor performance in the low-temperature regime, as shown in Section 3.

Fig. 6 shows species data for key intermediates measured by Zhang et al. [16] at 1 atm and Hashemi et al. [18] at 100 atm, both at φ = 0.5. The proposed model exhibits generally good agreement with experimental data, although slight discrepancies remain in predicting

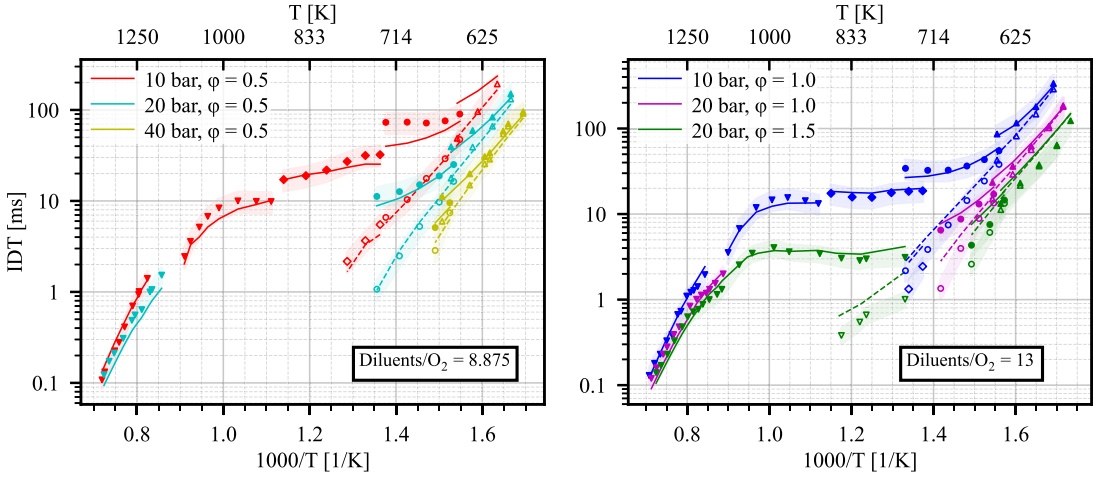

Fig. 5. Comparison of present model predictions with IDT measurements from this study. Shadow areas indicate the uncertainty in the measurements. Closed symbols denote main ignition; open symbols indicate first-stage ignition.

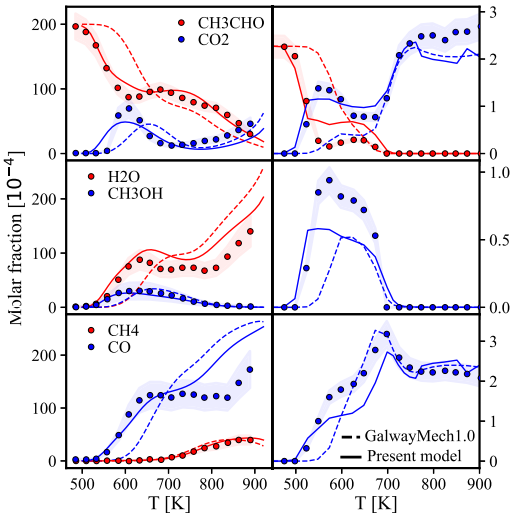

Fig. 6. Left column: JSR data from Zhang et al. [16] at φ = 0.5 and 1 atm. Right column: PFR data from Hashemi [18] at φ = 0.5 and 100 atm.

the formation of a few minor intermediates, such as methanol at high pressures. Despite of that, it achieves better performance than the original model, which systematically predicts the onset of fuel consumption and intermediate formation at higher temperatures than experimentally observed. Overall, the proposed model reasonably captures intermediate species formation and autoignition behavior over a wide range of conditions, demonstrating significant improvements over existing models from the literature, particularly in the high-pressure NTC regime relevant to modern engine applications.

6. Conclusions

In this work, acetaldehyde ignition delay times were measured over a wide range of conditions (p = 10–40 bar, φ = 0.5–1.5, T = 580–1413 K) using a shock tube and a rapid compression machine, providing critical high-pressure validation targets previously scarce in the literature. At low temperatures, existing kinetic models significantly underpredict reactivity at the studied conditions, despite showing reasonable agreement with previous low-pressure or dilute-reactant measurements. In contrast, better agreement was observed at high temperatures.

A comprehensive revision of the acetaldehyde submechanism within GalwayMech1.0 was conducted, including: (1) Rate coefficient modifications to enhance the closed-loop fuel consumption pathway of the acetyl peroxy radical, increasing reactivity at low temperatures, (2) updates to peroxyl species chemistry to better capture the separation between first-stage and main ignition times, and (3) revised fuel HAA rates to improve high-temperature predictions. Overall, the proposed model demonstrates improved accuracy across a wide range of conditions, outperforming existing literature models. Remaining uncertainties include model limitations in predicting the formation of a few minor intermediates and a lack of species data at high pressures. This study provides a solid foundation for future research on aldehyde oxidation at engine-relevant conditions.

Novelty and significance statement

The novelty of this research lies in the comprehensive analysis of acetaldehyde oxidation chemistry under enginerelevant conditions, a major intermediate in the combustion of several hydrocarbons. Novel ignition delay time data measured in a rapid compression machine and a shock tube under previously unexplored high-pressure conditions are presented. In addition, updates to the kinetic parameters within the acetaldehyde sub-mechanism of GalwayMech1.0 are proposed, addressing the limitations of existing kinetic models in reproducing the NTC behavior of this compound. This is significant because it allows the investigation of acetaldehyde oxidation pathways that have been previously underemphasized due to the low pressure or low initial fuel concentration conditions studied in the literature.

CRediT authorship contribution statement

Jesus Caravaca-Vilchez: Conceptualization, Data curation, Formal analysis, Investigation, Methodology, Software, Validation, Visualization, Writing – original draft, Writing – review & editing. **Malte Döntgen:** Investigation, Writing – review & editing. **Karl Alexander Heufer:** Conceptualization, Funding acquisition, Project administration, Supervision, Writing – review & editing.

Declaration of Generative AI and AI-assisted technologies in the writing process

During the preparation of this work the authors used DeepL Write in order to improve readability. After using this tool, the authors reviewed and edited the content as needed and take full responsibility for the content of the publication.

Declaration of competing interest

The authors declare that they have no known competing financial interests or personal relationships that could have appeared to influence the work reported in this paper.

Acknowledgment

The authors would like to recognize the funding support from the German Research Foundation (Deutsche Forschungsgemeinschaft, DFG) through the project number – 511644227.

Appendix A. Supplementary data

Supplementary material related to this article can be found online at https://doi.org/10.1016/j.proci.2025.105828.

References

[1] B. Chen, C. Togbé, Z. Wang, P. Dagaut, S.M. Sarathy, Jet-stirred reactor oxidation of alkane-rich FACE gasoline fuels, Proc. Combust. Inst. 36 (2017) 517–524.
[2] X. Fan, W. Sun, Y. Gao, N. Hansen, B. Chen, H. Pitsch, B. Yang, Chemical insights into the multi-regime low-temperature oxidation of di-n-propyl ether: Jet-stirred reactor experiments and kinetic modeling, Combust. Flame 233 (2021) 111592.
[3] J. Bourgalais, O. Herbinet, H.H. Carstensen, J. Debleza, G.A. Garcia, P. Arnoux, L.S. Tran, G. Vanhove, B. Liu, Z. Wang, M. Hochlaf, L. Nahon, F. Battin-Leclerc, Jet-stirred reactor study of low-temperature neopentane oxidation: A combined theoretical, chromatographic, mass spectrometric, and PEPICO analysis, Energy Fuels 35 (2021) 19689–19704.
[4] B. Liu, Q. Zhu, L. Zhu, C. Xie, Q. Xu, Z. Wang, Low-temperature oxidation of n-butanol in a jet-stirred reactor: Detailed species measurements and modeling studies, Combust. Flame 261 (2024) 113290.
[5] J. Caravaca-Vilchez, J. Liu, P. Wang, Y. Murakami, H.J. Curran, K.A. Heufer, Advancing the C_4 low-temperature oxidation chemistry through species measurements in a rapid compression machine, part a: 1-butene, Combust. Flame 272 (2025) 113833.
[6] J.F. Griffiths, S.M. Hasko, Two-stage ignitions during rapid compression: spontaneous combustion in lean fuel-air mixtures, Proc. R. Soc. A: Math. Phys. Eng. Sci. 393 (1984) 371–395.
[7] T. Tao, S. Kang, W. Sun, J. Wang, H. Liao, K. Moshammer, N. Hansen, C.K. Law, B. Yang, A further experimental and modeling study of acetaldehyde combustion kinetics, Combust. Flame 196 (2018) 337–350.
[8] R.D. Kern, H.J. Singh, K. Xie, A shock tube study of the thermal decompositions of acetaldehyde and ethylene oxide, AIP Conf. Proc. 208 (1990) 487–492.
[9] P. Dagaut, M. Reuillon, D. Voisin, M. Cathonnet, M. Mcguinness, J.M. Simmie, Acetaldehyde oxidation in a JSR and ignition in shock waves: Experimental and comprehensive kinetic modeling, CST 107 (1995) 301–316.

[10] S.-J. Won, J.-C. Ryu, J.-H. Bae, Y.D. Kim, J.-G. Kang, Shock-tube study of the oxidation of acetaldehyde at high temperature, Bull. Korean Chem. Soc. 21 (2000) 487–492.

[11] K. Yasunaga, S. Kubo, H. Hoshlkawa, T. Kamesawa, Y. Hidaka, Shock-tube and modeling study of acetaldehyde pyrolysis and oxidation, Int. J. Chem. Kinet. 40 (2008) 73–102.

[12] R. Mével, K. Chatelain, G. Blanquart, J.E. Shepherd, An updated reaction model for the high-temperature pyrolysis and oxidation of acetaldehyde, Fuel 217 (2018) 226–239.

[13] K.P. Shrestha, B.R. Giri, M. Adil, L. Seidel, T. Zeuch, A. Farooq, F. Mauss, Detailed chemical kinetic study of acetaldehyde oxidation and its interaction with NO_x, Energy Fuels 35 (2021) 14963–14983.

[14] E.W. Kaiser, C.K. Westbrook, W.J. Pitz, Acetaldehyde oxidation in the negative temperature coefficient regime: Experimental and modeling results, Int. J. Chem. Kinet. 18 (1986) 655–688.

[15] T. Tao, W. Sun, N. Hansen, A.W. Jasper, K. Moshammer, B. Chen, Z. Wang, C. Huang, P. Dagaut, B. Yang, Exploring the negative temperature coefficient behavior of acetaldehyde based on detailed intermediate measurements in a jet-stirred reactor, Combust. Flame 192 (2018) 120–129.

[16] X. Zhang, L. Ye, Y. Li, Y. Zhang, C. Cao, J. Yang, Z. Zhou, Z. Huang, F. Qi, Acetaldehyde oxidation at low and intermediate temperatures: An experimental and kinetic modeling investigation, Combust. Flame 191 (2018) 431–441.

[17] K. Hjuler, P. Glarborg, K. Dam-Johansen, Mutually promoted thermal oxidation of nitric oxide and organic compounds, Ind. Eng. Chem. Res. 34 (1995) 1882–1888.

[18] H. Hashemi, J.M. Christensen, P. Marshall, P. Glarborg, Acetaldehyde Oxidation at Elevated Pressure, 38, Proc. Combust. Inst., 2021, pp. 269–278.

[19] Y. Hidaka, S. Kubo, T. Hoshikawa, H. Wakamatsu, Shock-tube study of acetaldehyde pyrolysis, Shock Waves (2005) 603–608.

[20] S. Wang, D.F. Davidson, R.K. Hanson, High-temperature laser absorption diagnostics for CH_2O and CH_3CHO and their application to shock tube kinetic studies, Combust. Flame 160 (2013) 1930–1938.

[21] N. Leplat, J. Vandooren, Experimental investigation and numerical simulation of the structure of CH_3CHO/O_2/Ar flames at different equivalence ratios, CST 182 (2010) 436–448.

[22] T. Tao, W. Sun, B. Yang, N. Hansen, K. Moshammer, C.K. Law, Investigation of the chemical structures of laminar premixed flames fueled by acetaldehyde, Proc. Combust. Inst. 36 (2017) 1287–1294.

[23] M. Christensen, M.T. Abebe, E.J. Nilsson, A.A. Konnov, Kinetics of premixed acetaldehyde plus air flames, 35, Proc. Combust. Inst., 2015, pp. 499–506.

[24] X. Ren, H. Wu, R. Tang, Y. Cui, M. Wang, S. Cheng, Comprehensive reevaluation of acetaldehyde chemistry - part I: Assessment of important kinetic parameters and the underlying uncertainties, Appl. Energy Combust. Sci. 21 (2025) 100320.

[25] A. Ramalingam, K. Zhang, A. Dhongde, L. Virnich, H. Sankhla, H. Curran, A. Heufer, An RCM experimental and modeling study on CH_4 and CH_4/C_2H_6 oxidation at pressures up to 160 bar, Fuel 206 (2017) 325–333.

[26] M. Döntgen, A. Wildenberg, A. Heufer, Laser absorption shock tube study of C_1 to C_4 n-alkyl formate pyrolysis, in: 11th European Combustion Meeting, vol. 102, Rouen (France), 2023.

[27] H. Oguchi, K. Funabiki, A. Sato, An experiment on interaction of shock wave with multiple-orifice plate by means of snap-action shock tube, in: 10th Int. Symp. 106 107 Shock Tubes, 1975, pp. 386–391.

[28] J. Shepherd, Shock and detonation toolbox, 2024, https://shepherd.caltech.edu/EDL/Public-Resources/sdt/.

[29] D.G. Goodwin, R.L. Speth, H.K. Moffat, B.W. Weber, Cantera: An object-oriented software toolkit for chemical kinetics, thermodynamics, and transport processes, 2024, https://www.cantera.org.

[30] H. Minwegen, U. Burke, K.A. Heufer, An experimental and theoretical comparison of C_3–C_5 linear ketones, Proc. Combust. Inst. 36 (2017) 561–568.

[31] R.D. Büttgen, M. Preußker, D. Kang, S. Cheng, S.S. Goldsborough, G. Issayev, A. Farooq, H. Song, Y. Fenard, G. Vanhove, A.A.E.S. Mohamed, H.J. Curran, K.A. Heufer, Finding a common ground for RCM experiments. Part B: Benchmark study on ethanol ignition, Combust. Flame 262 (2024) 113338.

[32] C.J. Sung, H.J. Curran, Using rapid compression machines for chemical kinetics studies, PECS 44 (2014) 1–18.

[33] S. Zhou, A.A.E.S. Mohamed, S.S. Nagaraja, P. Wang, Y. Murakami, J. Liu, P.K. Senecal, H.J. Curran, An experimental and modeling study of hydrogen/n-decane blends, Combust. Flame 270 (2024) 113792.

[34] J. Liu, S. Zhou, P. Wang, Y. Murakami, A.A.E.-S. Mohamed, M. Raza, A. Nolte, K.A. Heufer, P.K. Senecal, H.J. Curran, An experimental and kinetic modeling study of the ignition of methane/n-decane blends, Combust. Flame 272 (2025) 113884.

[35] M. Pelucchi, K.P. Somers, K. Yasunaga, U. Burke, A. Frassoldati, E. Ranzi, H.J. Curran, T. Faravelli, An experimental and kinetic modeling study of the pyrolysis and oxidation of n-C_3-C_5 aldehydes in shock tubes, Combust. Flame 162 (2015) 265–286.

[36] M. Pelucchi, E. Ranzi, A. Frassoldati, T. Faravelli, Alkyl radicals rule the low temperature oxidation of long chain aldehydes, Proc. Combust. Inst. 36 (2017) 393–401.

[37] S. Wang, D.F. Davidson, R.K. Hanson, High temperature measurements for the rate constants of C_1–C_4 aldehydes with OH in a shock tube, Proc. Combust. Inst. 35 (2015) 473–480.

[38] R. Sivaramakrishnan, J.V. Michael, S.J. Klippenstein, Direct observation of roaming radicals in the thermal decomposition of acetaldehyde, J. Phys. Chem. A 114 (2010) 755–764.

[39] M. Altarawneh, A.H. Al-Muhtaseb, B.Z. Dlugogorski, E.M. Kennedy, J.C. MacKie, Rate constants for hydrogen abstraction reactions by the hydroperoxyl radical from methanol, ethenol, acetaldehyde, toluene, and phenol, J. Comput. Chem. 32 (2011) 1725–1733.

[40] J. Lee, C.J. Chen, J.W. Bozzelli, Thermochemical and kinetic analysis of the acetyl radical (CH_3CO) + O_2 reaction system, J. Phys. Chem. A 106 (2002) 7155–7170.

[41] J.P. Senosiain, S.J. Klippenstein, J.A. Miller, Pathways and rate coefficients for the decomposition of vinoxy and acetyl radicals, J. Phys. Chem. A 110 (2006) 5772–5781.

[42] A.O. Hui, M. Fradet, M. Okumura, S.P. Sander, Temperature dependence study of the kinetics and product yields of the HO_2 + $CH_3C(O)O_2$ reaction by direct detection of OH and HO_2 radicals using 2f-IR wavelength modulation spectroscopy, J. Phys. Chem. A 123 (2019) 3655–3671.

[43] M. Assali, C. Fittschen, Rate constants and branching ratios for the self-reaction of acetyl peroxy ($CH_3C(O)O_2$) and its reaction with CH_3O_2, Atmosphere 13 (2022) 186.

[44] S.A. Carr, D.R. Glowacki, C.H. Liang, M.T. Baeza-Romero, M.A. Blitz, M.J. Pilling, P.W. Seakins, Experimental and modeling studies of the pressure and temperature dependences of the kinetics and the OH yields in the acetyl + O_2 reaction, J. Phys. Chem. A 115 (2011) 1069–1085.

[45] L. Zhu, S. Panigrahy, S.N. Elliott, S.J. Klippenstein, M. Baigmohammadi, A.A.E.S. Mohamed, J.W. Hargis, S. Alturaifi, O. Mathieu, E.L. Petersen, K.A. Heufer, A. Ramalingam, Z. Wang, H.J. Curran, A wide range experimental study and further development of a kinetic model describing propane oxidation, Combust. Flame 248 (2023) 112562.

[46] P.D. Lightfoot, P. Roussel, F. Caralp, R. Lesclaux, Flash photolysis study of the CH_3O_2 + CH_3O_2 and CH_3O_2 + HO_2 reactions between 600 and 719 K: unimolecular decomposition of methylhydroperoxide, J. Chem. Soc. Faraday Trans. 87 (1991) 3213–3220.

[47] D. Johnson, D.W. Price, G. Marston, Correlation-type structure activity relationships for the kinetics of gas-phase RO_2 self-reactions and reaction with HO_2, Atmos. Environ. 38 (2004) 1447–1458.